

# Pore confinement effects and stabilization of carbon nitride oligomers in macroporous silica for photocatalytic hydrogen production

Sha Qiao,<sup>a</sup> Robert W. Mitchell,<sup>a</sup> Ben Coulson,<sup>a</sup> Danielle V. Jowett,<sup>a</sup> Benjamin R. G. Johnson,<sup>b</sup> Rik Brydson,<sup>b</sup> Mark Isaacs,<sup>c</sup> Adam F. Lee<sup>c</sup> and Richard E. Douthwaite<sup>\*,a</sup>

<sup>a</sup>Department of Chemistry, University of York, Heslington, York, YO10 5DD, UK

<sup>b</sup>Institute for Materials Research, School of Chemical and Process Engineering, University of Leeds, Leeds LS2 9JT, UK

<sup>c</sup>European Bioenergy Research Institute, Aston University, Birmingham B4 7ET, UK

## Abstract

An ordered macroporous host (mac-SiO<sub>2</sub>) has been used to prevent aggregation of layered photocatalysts based on carbon nitride. Using typical carbon nitride synthesis conditions, cyanamide was condensed at 550 °C in the presence and absence of mac-SiO<sub>2</sub>. Condensation in the absence of mac-SiO<sub>2</sub> results in materials with structural characteristics consistent with the carbon nitride, melon, accompanied by ca. 2 wt% carbonization. For mac-SiO<sub>2</sub> supported materials, condensation occurs with greater carbonization (ca. 6 wt%). On addition of 3wt% Pt cocatalyst photocatalytic hydrogen production under visible light is found to be up to 10 times greater for the supported composites. Time-resolved photoluminescence spectroscopy shows that excited state relaxation is more rapid for the mac-SiO<sub>2</sub> supported materials suggesting faster electron-hole recombination and that supported carbon nitride does not exhibit improved charge separation. CO<sub>2</sub> temperature programmed desorption indicates that enhanced photoactivity of supported carbon nitride is attributable to an increased surface area compared to bulk carbon nitride and an increase in the concentration of weakly basic catalytic sites, consistent with carbon nitride oligomers.

## 1. Introduction

The specific activity (per unit mass) of a heterogeneous catalyst can be increased by controlling morphology, typically by increasing the geometric surface area. For heterogeneous photocatalysts there are the additional considerations of photon absorption and subsequent electron/hole migration that precede surface reactions.[1] In the absence of significant surface reconstruction, increasing the specific surface area of a photocatalyst typically enhances the number of catalytically active sites, while suppressing bulk electron-hole recombination. High surface areas can also be stabilized by dispersing active phases

onto thermally/mechanically robust supports in order to retard aggregation.[2-5] Such supports may possess non-planar morphologies, featuring meso- or macroporosity which further increases the specific activity of resulting composites. With respect to light absorption, morphology can also modify absorption by e.g. increasing the path length via scattering or photonic effects.[6-9]

Materials able to mediate photochemical reactions are likely to make significant contributions to future energy needs and associated chemical technologies.[1, 10] The vast majority of photocatalysts are based on semiconductor inorganic oxides, principally because they exhibit significant photostability, and their structural diversity allows photon absorption and catalysis to be modified by cation and anion substitution. However, carbon based materials have more recently come to prominence as organic-inorganic hybrids, incorporating e.g. carbon nanotubes, graphene and quantum dots.[11-17] In addition, metal-free graphitic carbon nitride (g-C<sub>3</sub>N<sub>4</sub>) has been reported as a photocatalyst for the sacrificial production of dihydrogen from water, although typically metal co-catalysts are also required.[18, 19]

The idealized structure of g-C<sub>3</sub>N<sub>4</sub> is not realized when using the most common synthetic procedures involving hydrogen-containing precursors.[18, 20-26] Synthesis is typically achieved via thermal decomposition of molecular precursors such as cyanamide, dicyanamide, melamine or urea. For example cyanamide (**1**) (Fig. 1) is heated to eliminate ammonia to generate the heptazine melem (**2**) with the characteristic tris-*s*-triazine moiety. This can be further condensed to melon, which may have several isomeric forms[27-29] such as (**3**) and, conceptually at least, ultimately to the idealized composition g-C<sub>3</sub>N<sub>4</sub>, which contains infinite 2-D sheets. The local and long-range structure can lead to similar analytical data from common methods of characterization, and hence establishing the true composition and structure necessitates application of a broad range of techniques.[18, 20-22, 30] Nevertheless, g-C<sub>3</sub>N<sub>4</sub> and carbon nitride (CN) are used as descriptors for a range of compositions, which differ in their extent of condensation, CHN composition, and possibly oxygen content.[24] Indeed it has been shown that using hydrogen containing precursors such as cyanamide, the resulting 'carbon nitride' product synthesized above 500 °C is predominantly melon (**3**), which also has several potential structures,[22, 28, 31] and that continued heating leads to carbonization in addition to further polymerisation.[20] This is reflected in the colour of the resultant carbon nitride, which ranges from light yellow to brown. Moreover, a C:N ratio is often the principal evidence of composition, while the H content is ignored despite CHN contents from combustion analysis falling below 95 %. Many materials described as g-C<sub>3</sub>N<sub>4</sub> in the literature are in likelihood mainly melon[32]

and/or also contain oxygen defects[33] and are partially carbonized, which is often observed in XPS but simply assigned to spectral impurities.[20, 34]

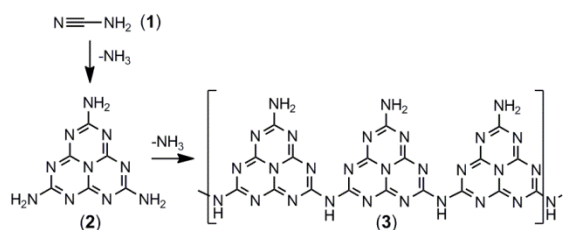


**Fig. 1.** Elimination of ammonia from cyanamide (1) leading to condensed structures melon (2) and melon (3).

With respect to morphology, the specific photocatalytic activity of carbon nitrides has been improved by increasing the surface area via the introduction of mesopores, [22, 35-41] nanosheet exfoliation,[42-44] and synthesis of morphologies containing a range of nano- to macroscopic structural features.[39, 45-53] The specific activity of these morphologies is typically increased by 3–10 fold compared to the bulk carbon nitride under visible light ( $\geq 400$  nm) illumination. Of direct relevance to this work, carbon nitrides have also been integrated with oxides such as silica and titania to form photocatalytic composites for dye degradation, or to support catalytic nanoparticles.[54-60]

Herein we describe the use of ordered macroporous silica (mac-SiO<sub>2</sub>) as a support for carbon nitride oligomeric nanosheets comprising primarily melon-like composition and structure. Aggregation into bulk morphologies is hindered by the macroporous support, stabilizing high surface area forms. Furthermore, photoluminescence, XPS and CO<sub>2</sub> temperature programmed desorption show that the mac-SiO<sub>2</sub> support modifies condensation of the cyanamide precursor, favouring less condensed structures and greater carbonization at lower CN concentrations. Photocatalytic hydrogen production over the platinumized CN@mac-SiO<sub>2</sub> nanocomposites was 10 times greater than the unsupported carbon nitride.

## 2. Experimental

### 2.1. Materials and characterisation methods

Cyanamide (99 %), tetraethyl orthosilicate (99 %), and chloroplatinic acid hexahydrate (37 % Pt) were supplied by Sigma Aldrich and used as received. Polystyrene templates were prepared by a literature method.[61, 62] PXRD of bulk carbon nitride and CN@mac-SiO<sub>2</sub> composites were analysed using a Bruker-AXS D8 Avance instrument fitted with a Lynx eye detector. Patterns were

recorded using Cu  $K_{\alpha}$  radiation ( $\lambda = 1.5406 \text{ \AA}$ ), scanning in the range  $10 - 70^{\circ} 2\theta$ , with a  $0.02^{\circ}$  step size and with each data point collected for 0.1 s. FT-IR spectra were measured on a Thermo Nicolet Avatar 370 FT-IR with a desiccant air dryer to remove  $\text{CO}_2$ . KBr was used to disperse the sample and the mixture was pressed into a 13 mm disk using an hydraulic press. UV-visible diffuse reflectance and absorbance spectra were obtained using an Ocean Optics Inc. HR2000+ High Resolution Spectrometer, with DH-2000-BAL Deuterium/Helium light source (200 – 1100 nm) and R400-7-UV-Vis reflection probe. Spectra were averaged over 10 scans with a boxcar width of 30. SEM images were acquired on an FEI Sirion scanning electron microscope operated at 5 kV. Powdered samples were supported on an adhesive carbon tab mounted on an aluminium stub. Transmission electron microscopy (TEM) analyses including EELS and EDX were obtained using a JEOL JEM-2010 TEM, a FEI CM200 field emission TEM with Gatan EELS imaging filter and a FEI Tecnai FT20 field emission TEM all operating at 200 kV. Samples were dispersed in methanol, ground in a mortar and pestle and sonicated for 5 min before drop casting onto holey carbon film supported on a copper grid and dried in air. Nitrogen adsorption/desorption porosimetry was used to calculate the Brunauer Emmett Teller (BET) surface area of the samples. Samples were dried under nitrogen at  $150^{\circ}\text{C}$  for 6 h prior to measurement at 77.4 K using a Micromeritics Tristar 3000 instrument. Surface area measurements were calculated from data points in the 0.05 to 0.3  $P/P_0$  region.[63] CN surface areas were determined by selective  $\text{CO}_2$  chemisorption on a Quantachrome ChemBET 3000 surface area analyser relative to a  $\text{MgCO}_3$  reference; samples were degassed under 120 mL/min flowing He at  $120^{\circ}\text{C}$  for 1 h prior to  $\text{CO}_2$  saturation at  $40^{\circ}\text{C}$  and subsequent desorption under a temperature ramp of  $8^{\circ}\text{C min}^{-1}$ . CHN analysis of solid samples was obtained by combustion at  $1500^{\circ}\text{C}$  in He gas using an Exeter Analytical CE-440 analyser. Solid state NMR data were acquired using a Bruker Avance III HD 400 spectrometer equipped with a 9.4 T wide-bore magnet and a 4 mm MAS probe. Spectra were referenced externally to tetramethylsilane. XPS spectra were acquired using a Kratos Axis HSi XP spectrometer equipped with a charge neutralizer and a monochromated aluminium  $K_{\alpha}$  source (1486.7 eV). Spectra were recorded at normal emission using a pass energy of 40 under a vacuum of  $10^{-10}$  Torr. Curve fitting was performed using CasaXPS software version 2.3.16 and energy calibrated to the carbon 1s peak at 284.6 eV, employing Gaussian-Lorentz peak shapes and a Shirley background. Steady state photoluminescence maps were acquired using a F-4500 FL Spectrophotometer (Hitachi) in 3D-scan mode with excitation and emission between 200 and 700 nm and excitation and emission slit widths of 2.5 and 5 nm, respectively. Time-resolved photoluminescence data were recorded using a PLS980 (Edinburgh Photonics) by time-correlated photon counting. Excitation was achieved using a pulsed LED (380 nm) and emission was monitored at 480 nm. Data were fit using reconvolution to a three term exponential in PL980 software.

## 2.2. Synthesis

### 2.2.1. Synthesis of mac-SiO<sub>2</sub>.

Tetraethylorthosilicate (3 mL, 13.4 mmol), ethanol (2 mL), water (1.5 mL) and 1 M HCl (0.5 mL) were mixed and stirred for 15 min. The solution was transferred via pipette onto a powdered polystyrene template (1 g) supported by a filter frit and soaked for 30 min. Excess solution was removed under reduced pressure and the impregnated template was dried at room temperature for 24 h prior to calcination at 550 °C (1 °C / min) for 10 h, to yield mac-SiO<sub>2</sub> (150 mg) as a pale blue powder due to the photonic structure.

### 2.2.2. Synthesis of bulk carbon nitride/melon (**4**).[26]

Cyanamide (150 mg, 3.5 mmol) was placed in a 10 mL glass vial and heated under a flow of nitrogen to 550 °C at a rate of 2.5 °C min<sup>-1</sup> and held for 4 h. The resulting solid was cooled to room temperature to give a yellow-orange solid (79 mg, yield by mass 53 %). The solid was ground into a fine powder using a pestle and mortar.

### 2.2.3. Synthesis of CN@mac-SiO<sub>2</sub> (**5** – **7**).

Cyanamide (40, 70 and 120 mg) was dissolved in ethanol (2 mL) and the solution added to a 10 mL glass vial containing mac-SiO<sub>2</sub> (120 mg). The solvent was evaporated at 60 °C and then the solid mixture heated under a flow of nitrogen to 550 °C at a rate of 2.5 °C min<sup>-1</sup> and held for 4 h. The solid was cooled to room temperature to give CN@mac-SiO<sub>2</sub> (**5** – **7**). Colours ranged from pale yellow (**5**) to yellow (**7**) for increasing masses of cyanamide.

### 2.2.4. Platinum addition to **4** – **7**.

The materials **4** – **7** were decorated with 3 wt % Pt based on the C<sub>x</sub>N<sub>y</sub> content of the composites determined by elemental analysis. Pt from a stock solution (10 mM) of chloroplatinic acid hexahydrate (**4** (1154 μL), **5** (76 μL), **6** (148 μL), **7** (325 μL)) was made up to 2 mL with deionized water and added to **4** – **7** (75 mg) to give a mixture. The volatiles were removed by heating at 90 °C in air and the subsequent solid heated to 200 °C at a ramp rate of 1 °C min<sup>-1</sup> under a flow (60 mL min<sup>-1</sup>) of hydrogen and held at 200 °C for 1 h to give dull yellow powders (Pt-**4** – **7**). Pt (325 μL of a 10 mM stock solution) was also added to mac-SiO<sub>2</sub> (75 mg) using an analogous method with the same Pt loading as used for **7** to give a grey powder.

## 2.3. Photocatalysis

The apparatus used for photoreactions has been described previously.[64] Typically 70 mg of photocatalyst was used except where stated otherwise (Table 2). Reactions were performed in a solution of water and triethanolamine in 9:1 vol % (50 mL) and the apparatus maintained at a temperature of 40 °C. Illumination was performed using a 300 W Xe lamp fitted with a 15 cm IR filter and a wideband AlMgF<sub>2</sub> coated mirror followed by a 40 nm long band pass filter. Gas analysis was performed using a Shimadzu Corporation GC-2014. Gases were separated on a 25 cm long column packed with 5 Å molecular sieves and detection was performed using a thermal conductivity detector (TCD). The gas samples were analysed using the following conditions; 20 mL/min flow rate of Ar gas, 90 °C column temperature and 120 °C detector temperature. Under these conditions the retention time of H<sub>2</sub> is 1.5 min.

### 3. Results

#### 3.1. Synthesis

Ordered macroporous silica (mac-SiO<sub>2</sub>) was prepared using an established polystyrene sphere templating methodology.[62] Polystyrene spheres of 500 nm diameter were ordered into an fcc array under centrifugation. The interstitial volume of the polystyrene template was impregnated with Si(OEt)<sub>4</sub> which was hydrolyzed and subsequently calcined in air at 550 °C to burn off the template and give mac-SiO<sub>2</sub>. [61]

For control experiments carbon nitride (**4**) was prepared using an established procedure from cyanamide (**1**). [20, 26] Cyanamide was selected because other common potential precursors such as dicyanamide and melamine are much less soluble in common solvents which prevents easy incorporation into mac-SiO<sub>2</sub> (*vide infra*). The exact composition and structure of ‘carbon nitride’ has been discussed since Leibig’s initial report in 1834 [65] and recent evidence suggests that the pyrolysis of hydrogen containing molecular precursors at typical temperatures between 450 and 650 °C leads to melon (**3**) being the predominant component. [20, 24]

Using an analogous procedure, pyrolysis of cyanamide was also undertaken after being mixed with mac-SiO<sub>2</sub>. Cyanamide was dissolved in ethanol and added to mac-SiO<sub>2</sub> powder before evaporating the ethanol at 60 °C followed by pyrolysis at 550 °C. It should be noted that cyanamide has a boiling point of 260 °C with decomposition which results in mass loss in excess of that expected from only the elimination of ammonia, and has been observed for porous carbon nitrides prepared using cyanamide and SiO<sub>2</sub> templates. [66, 67] Three different masses of cyanamide (40, 70 and 120 mg) were added to mac-SiO<sub>2</sub> (120 mg) to

give CN@mac-SiO<sub>2</sub> (**5** – **7**) as pale yellow to yellow powders. Preliminary experiments showed that lower masses did not give detectable nitrogen content by elemental analysis for the resulting composite, presumably due to complete evaporation, and greater masses of cyanamide led to significantly reduced surface area (*vide infra*). For photocatalytic experiments, a cocatalyst of 3 wt% Pt, based on the CN content, was added to **5** – **7**, and as a control Pt was also added to mac-SiO<sub>2</sub>.

## 2.2. Characterisation

Products were characterized using a combination of combustion elemental analysis, Powder X-ray diffraction (PXRD), Scanning Electron Microscopy (SEM), Analytical Transmission Electron Microscopy (TEM), nitrogen adsorption porosimetry (BET), temperature programmed desorption of CO<sub>2</sub>, X-ray photoelectron spectroscopy (XPS), Infra-Red (IR), Diffuse Reflectance UV-Vis (DRUVS), <sup>13</sup>C CP-MAS solid state NMR, and steady state and time-resolved photoluminescence spectroscopies.

SEM of mac-SiO<sub>2</sub> showed an ordered morphology with the inverse opal structure derived from the fcc template (Fig. 2a). Polystyrene spheres of 500 nm diameter gave a macroporous structure with 420 nm diameter pores due to densification of the walls on calcination. The preparation of mac-SiO<sub>2</sub> has been described previously and the characterization data is consistent with earlier reports.[61, 62] PXRD showed that the walls were amorphous with a very broad peak centred at 22°, while elemental analysis only detected trace carbon (Table 1) indicating full removal of the polystyrene spheres. The surface area of mac-SiO<sub>2</sub> was 69 ± 1 m<sup>2</sup> g<sup>-1</sup> via nitrogen porosimetry. It should be noted that the macropore dimensions do not give rise to adsorption-desorption hysteresis or mass-transport limitations in solution processes and there is no evidence of micro-mesoporosity.[68]

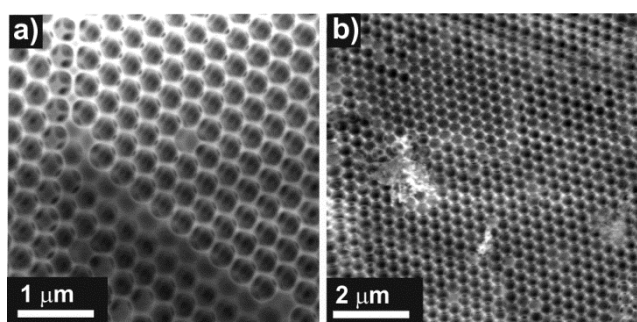


**Fig. 2.** a) SEM of mac-SiO<sub>2</sub>; b) SEM of CN@mac-SiO<sub>2</sub> (**5**).

Elemental analysis (Table S1) suggests that melon (**3**) is the predominant constituent of **4**. The stoichiometry of melon is C<sub>2</sub>H<sub>1</sub>N<sub>3</sub> equating to a C:N ratio of 0.660 versus 0.750 for

fully condensed g-C<sub>3</sub>N<sub>4</sub>. The stoichiometry of **4** produced here (normalized to C<sub>2</sub>) is C<sub>2</sub>H<sub>1.13</sub>N<sub>2.97</sub> and the C/N ratio is 0.673 (Table 1). For composites **5 – 7** an increasing CHN content with cyanamide precursor addition is observed (Table 1). It should be noted that an unknown proportion of the hydrogen is associated with surface hydroxyl groups in the mac-SiO<sub>2</sub> framework. Elemental analysis initially suggests greater polymerization occurs in **5 - 7** than the bulk material, however the C/N ratios remain below those for g-C<sub>3</sub>N<sub>4</sub>.

**Table 1.** Elemental analysis, CHN stoichiometry normalized to C<sub>2</sub>H<sub>x</sub>N<sub>y</sub>, and surface areas of mac-SiO<sub>2</sub> and bulk CN (**4**) and CN@mac-SiO<sub>2</sub> (**5 – 7**)

sample	CHN wt%	C <sub>2</sub> H <sub>x</sub> N <sub>y</sub>	C:N	Total surface area <sup>a</sup> (m <sup>2</sup> .g <sup>-1</sup> )	CN surface area <sup>b</sup> (m <sup>2</sup> .g <sup>-1</sup> )
mac-SiO <sub>2</sub>	0.13	C <sub>0</sub> H <sub>0.13</sub> N <sub>0</sub>	-	69	
<b>4</b>	98.0	C <sub>2</sub> H <sub>1.13</sub> N <sub>2.97</sub>	0.673	3	
<b>5</b>	6.6	C <sub>2</sub> H <sub>2.00</sub> N <sub>2.82</sub>	0.710	56	30
<b>6</b>	12.8	C <sub>2</sub> H <sub>2.31</sub> N <sub>2.87</sub>	0.700	54	38
<b>7</b>	28.2	C <sub>2</sub> H <sub>1.49</sub> N <sub>2.85</sub>	0.702	50	35

<sup>a</sup> From N<sub>2</sub> adsorption. <sup>b</sup> From CO<sub>2</sub> chemisorption.

PXRD of **4** exhibits three major broad peaks at 13.1, 17.5 and 27.0 ° (Fig. S2a) commonly observed for carbon nitrides. The latter corresponds to an interplanar spacing of 0.329 nm, compared to 0.326 nm reported for the 2-D structure of carbon nitrides,[18, 20, 22] and the powder pattern is consistent with a structural model of melon recently proposed.[29] This structure comprises buckled chains of tris-*s*-triazine moieties idealized as **3** (Fig. 1). For **5 - 7**, PXRD showed no peaks attributable to CN resolvable from the amorphous mac-SiO<sub>2</sub> (Fig. S2b), however for **7** a shoulder becomes evident at 27° 2θ consistent with **4**. Selected area electron diffraction in the TEM suggested a turbostratic layered structure for **4** and **7** consistent with the X-ray data (Fig. S3a).

IR spectroscopy of **4** shows characteristic peaks at 1100 – 1600 cm<sup>-1</sup> attributable to C-N stretching modes and at 810 cm<sup>-1</sup> characteristic of the *s*-triazine breathing mode showing that polymerization has occurred (Fig. S4). [18, 20, 22] Composites **5 - 7** show a superposition of features attributable to mac-SiO<sub>2</sub> and **4**, with the latter bands between 1100 – 1600 cm<sup>-1</sup> increasing in intensity with cyanamide loading (Fig. S4).

<sup>13</sup>C CP-MAS solid state NMR (Fig. 3) provides more direct evidence to suggest that melon (**3**) is the predominant constituent. Direct excitation does not show significant intensity, however cross-polarization experiments show two peaks at δ 157 and 164 ppm, which have previously been attributed to CN<sub>3</sub> and CN<sub>2</sub>(NH<sub>x</sub>) moieties, again consistent with the melon structure.[20, 55, 69] <sup>13</sup>C CP-MAS NMR spectra of **5 - 7** (Fig. 3) show two

signals at  $\delta$  157 and 164 ppm, essentially identical to **4**, indicating a very similar local structure for all materials.

SEM of **4** shows particles with sheet-like morphology and surface pores (Fig. S5a) but the surface area of only  $3 \text{ m}^2 \cdot \text{g}^{-1}$  determined from  $\text{N}_2$  adsorption porosimetry (Table 1) suggests a condensed structure. SEM of **5 – 7** (Fig. 2b and S5b) confirms retention of the macroporous structure following cyanamide pyrolysis, however small patches of a new phase are now evident and would logically appear associated with cyanamide degradation/polymerization. The underlying parent macropore architecture remains visible for all cyanamide loadings, indicating that coverage is throughout the macropores and is not confined to the outer surface.

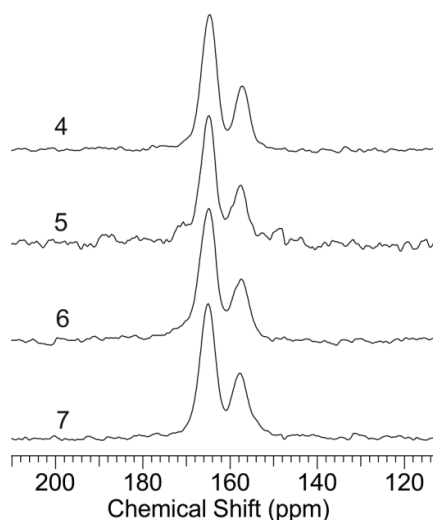


**Fig. 3.**  $^{13}\text{C}$  CP-MAS NMR of bulk CN (**4**) and CN@mac-SiO<sub>2</sub> (**5 – 7**).

DRUVS and absorption spectroscopy also show features typical of carbon nitride with a band edge at 470 nm, which from a Tauc plot yield an indirect band gap of 2.70 eV (Fig S6a and b). This is consistent with that of 2.6 eV typically reported for carbon nitrides and g-C<sub>3</sub>N<sub>4</sub>. [18, 20, 22] The ordered periodic structure of the mac-SiO<sub>2</sub> support allows additional insight into the homogeneity of the composites from examination of the photonic optical properties. DRUVS shows characteristic stop band consistent with a photonic macroporous structure (Fig. 4). The optical Bragg reflections at 380 and 610 nm arise from the structural order of the macropores and the resulting periodic modulation in the refractive index between the walls and the voids. [70-72] Addition of species within the macropores possessing a different refractive index will therefore modify the stop band position, with the distribution of in-pore species influencing both stop band intensity and width. If the additional species is not homogeneously distributed and commensurate with the macropore periodicity, then a reduction in stop band intensity and increased bandwidth are

observed.[61, 70, 73] DRUVS spectra for **5** – **7** (Fig. 4) shows that CN addition does not significantly change the stop band positions at 380 and 610 nm, however their intensity is significantly reduced for **6** and **7**, indicating that CN species are formed inside the macropores during cyanamide pyrolysis and do not conformally coat the surface of mac-SiO<sub>2</sub>.

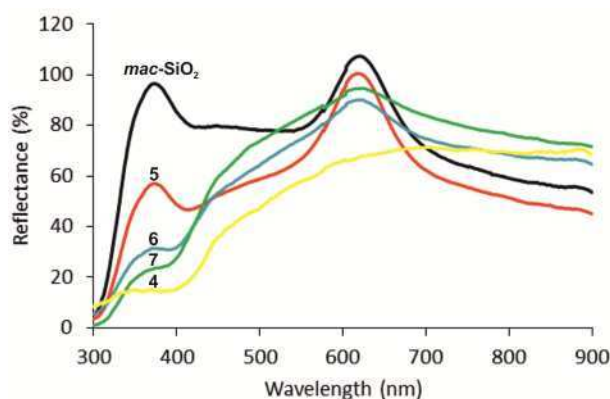


**Fig. 4.** DRUVS of mac-SiO<sub>2</sub> and bulk CN (**4**) and CN@mac-SiO<sub>2</sub> (**5** – **7**).

The measured N<sub>2</sub> adsorption surface areas of **5** – **7** are less than the parent mac-SiO<sub>2</sub> ranging from 56 (**5**) to 50 m<sup>2</sup> g<sup>-1</sup> (**7**) (Table 1). Previous studies of macroporous materials comprised of microcrystalline walls and of a similar periodicity possessed surface areas of 20 – 30 m<sup>2</sup> g<sup>-1</sup>. [61] Higher areas of 60 - 90 m<sup>2</sup> g<sup>-1</sup> for mac-SiO<sub>2</sub> thus imply N<sub>2</sub> accessible surface area within the amorphous walls. [61] In the present work, it is clear that CN in-pore incorporation does not block macropore accessibility to nitrogen although it is not possible to quantify the relative contributions to the total surface area of mac-SiO<sub>2</sub> and CN from N<sub>2</sub> adsorption. CO<sub>2</sub> chemisorption was used to selectively titrate the basic CN component of **5** - **7** and estimate the relative CN surface area (Fig. S7, Table 1). An almost linear increase in area with CN content gives similar surface area per gram of CN, indicating that essentially all of the framework-incorporated nitride remains accessible. CO<sub>2</sub> desorption temperatures and hence solid basicity increased from composites **5** → **7**, indicating differing surface speciation which have previously been assigned to pyridyl- and amine-like terminated CN surfaces (Fig. 1, **3**). [18, 74]

TEM (Fig. 5a) and scanning TEM–energy dispersive X-ray analysis (STEM-EDX) mapping (Fig. 5b-f) of **5** shows that the CN is distributed throughout the macroporous structure. Coverage is not completely homogeneous and the CN sheets are partially separated from the walls of the macroporous host as indicated in the DRUVS data.

XPS measurements (Fig. 6) of **4** gave signals typical of carbon nitrides. The C 1s spectra comprised components with binding energies of 284.6 eV, 286.0 eV and 288.1 eV,

consistent with literature assignments for carbon nitride[75] or carbonaceous (graphitic) impurity,[22, 33, 45, 76, 77]  $C\equiv N$  moieties,[76] and CNC coordination in the triazine ring[22, 33, 45, 76, 77] respectively. Corresponding N 1s spectra exhibited components at 398.5 eV, 400 eV and 401.1 eV, assigned to CNC (398.7 eV),  $N_3C$  (400.1 eV) and CNH (401.4 eV) groups.[22, 33, 45, 76, 77] The CN@mac-SiO<sub>2</sub> composites (**5** - **7**) all exhibited the same three C 1s and N 1s spectral features of the bulk carbon nitride, but also possessed additional features at 287.0 eV and 397.4 eV indicative of an aliphatic nitrile chemical environment. The proportion of this nitrile species reaches 12 atom% of the total surface carbon species for **7**, suggesting that the macroporous framework inhibits complete pyrolysis of high precursor concentrations. However, there is a clear evolution of the overall spectral envelope and fitted components of the CN@mac-SiO<sub>2</sub> composites in Fig. 6 towards that of **4** with increasing cyanamide loading.

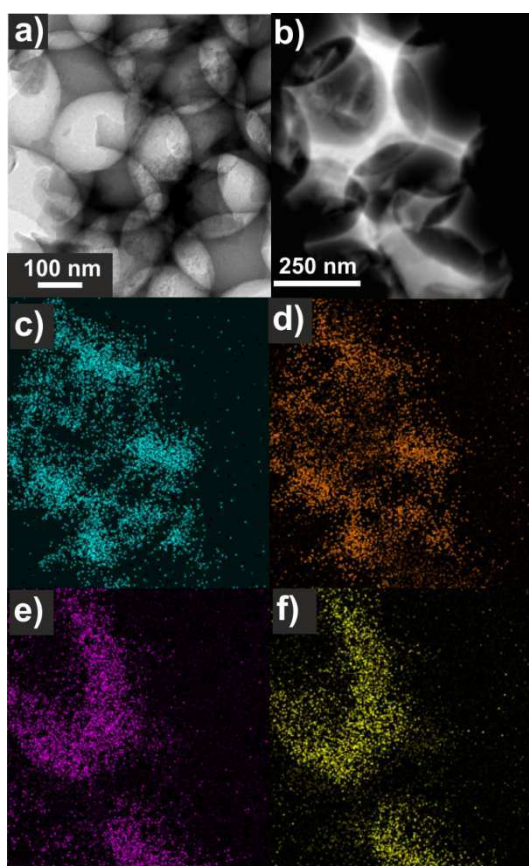


**Fig. 5.** TEM, STEM image and EDX maps of CN@mac-SiO<sub>2</sub> (**5**). a) TEM image; b) STEM image; c) silicon; d) oxygen; e) carbon; f) nitrogen element maps.

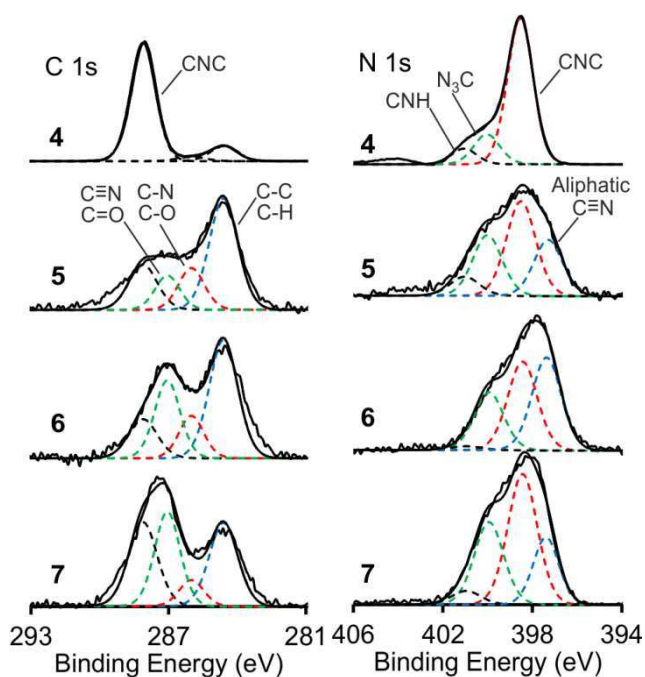


**Fig. 6.** Background-subtracted, fitted C 1s and N 1s XP spectra of bulk CN (**4**) and CN@mac-SiO<sub>2</sub> (**5 – 7**).

Surface compositional analysis (Table S2) yields a C:N atomic ratio of 0.9 and comparable to that measured by Electron Energy Loss Spectroscopy (EELS) of 1.0 (Fig. S8). Both carbon and nitrogen EELS K-edges (~285 eV and 400 eV respectively) exhibited leading  $\pi^*$  features evidencing  $sp^2$ -hybridized bonding (Fig. S7) in agreement with previous studies.[22] However, XPS of **5 - 7** revealed significant deviation from the bulk C:N stoichiometry, decreasing from 2.2→1.1 with increasing cyanamide loading, in contrast to the EELS values which showed only slight variation between materials ( $\pm 0.1$ ) and little evidence for oxidation. This discrepancy suggests that a small fraction of cyanamide pyrolysis products may undergo partial oxidation through reaction with silanols and concomitant surface segregation (vide infra).

### 3.3. Photocatalysis

Photocatalytic hydrogen production was conducted under typical conditions reported for ‘carbon nitride’ materials, using a 300 W Xe lamp and 420 nm filter in a 10 v/v% aqueous solution of triethanolamine, which acts as a sacrificial reductant. We found that compounds **4 – 7** did not mediate hydrogen production under irradiation (Fig. S9a) and that addition of a Pt co-catalyst was required for hydrogen production. To mac-SiO<sub>2</sub> and **4 – 7** was added 3 wt% Pt, based on the CN wt% (Pt-**4 – 7**), which has been found to optimize hydrogen

production for CN materials and is the most common loading investigated.[26] TEM analysis (Fig. S3b and S3c) showed Pt nanoparticles between 2 - 5 nm in diameter dispersed throughout the composite, however it was not possible to identify whether Pt nanoparticles were preferentially supported on mac-SiO<sub>2</sub> or CN. The composite was also examined after photocatalysis, confirming that Pt nanoparticles were retained with no evidence for sintering (Fig. S3d and S3e).

Pt-4 – 7 mediate photoactivated hydrogen production (Fig. 7 and Table 2). For Pt-5, a photoreaction was run collecting a total of >400 μmol of hydrogen, which is significantly greater than the amount of hydrogen present within 5 or that could arise from water derived photooxidation of the CN content (~30 μmol) confirming that its production must be catalytic. Control experiments showed no hydrogen production either in the absence of light, or when illuminating Pt@mac-SiO<sub>2</sub> for 6 h, indicating that hydrogen production is photoactivated and that both CN and Pt are required for photoactivity. For Pt-4, we found that hydrogen production steadily slowed by 10 – 20 % over tens of hours (Fig. S9b), which is consistent with related literature reports. A similar deactivation was observed for Pt-5 – 7 (Fig. S9c), which may also potentially be prone to CN delamination and subsequent aggregation.

The photoactivity of Pt-5 – 7 (Fig. 7 and Table 2) shows that dispersing CN onto mac-SiO<sub>2</sub> increased the CN specific activity for hydrogen production. It should be noted that the total surface area of the composites 5 - 7 comprises contributions from both CN and mac-SiO<sub>2</sub>, which cannot be readily deconvoluted using N<sub>2</sub> adsorption. Therefore hydrogen production is normalized against mass as a specific (per g) activity, which is most commonly used when surface area cannot be determined.[78, 79]

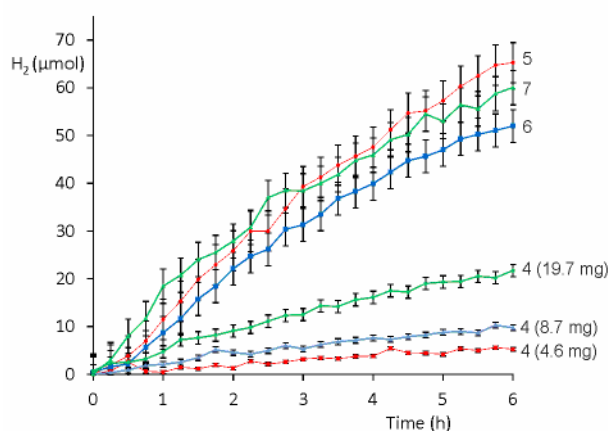


**Fig. 7.** Photoactivated hydrogen production over 70 mg Pt-5 – 7 and control experiments using equivalent masses of Pt-4.

**Table 2.** Photocatalytic hydrogen production from Pt@mac-SiO<sub>2</sub> and Pt-4 – 7.

Sample <sup>a</sup>	H <sub>2</sub> ( $\mu\text{mol h}^{-1} \text{g}^{-1} \text{CN}$ )
Pt@mac-SiO <sub>2</sub> (70 mg)	0
Pt-4 (40 mg)	200
Pt-5 (70 mg (4.6 mg CN))	2250
Pt-4 (4.6 mg)	180
Pt-6 (70 mg (8.7 mg CN))	960
Pt-4 (8.7 mg)	190
Pt-7 (70 mg (19.7 mg CN))	510
Pt-4 (19.7 mg)	180

<sup>a</sup> Conditions: 300 W Xe lamp, 420 nm filter, 50 mL 10 v% triethanolamine in water. The catalyst mass is given in brackets and for Pt-5 - 7 also the mass of CN in the composite which was calculated from elemental analysis (Table S1).

The loading dependence of Pt-4 was also explored, enabling a direct comparison between bulk melon and the dispersed CN present within Pt-5 – 7. The rate of hydrogen production of 4 was essentially independent of catalyst loading over the range explored in this study, at ca. 180  $\mu\text{mol.h}^{-1}.\text{g}^{-1}$ . This is in reasonable agreement with values of 100-200  $\mu\text{mol.h}^{-1}.\text{g}^{-1}$  reported for other control samples of carbon nitrides measured under the same illumination conditions, reaction solution, and Pt loading.[26, 36, 42, 80] In contrast, the specific activity of Pt-5 was 2250  $\mu\text{mol.h}^{-1}.\text{g}^{-1}$  during the first 6 h of reaction, an 11-fold rate enhancement relative to an equivalent mass of Pt-4 present in Pt-5. Composites Pt-6 and Pt-7 also exhibited 5- and 3-fold rate-enhancement respectively relative to equivalent masses of Pt-4; the progressive decrease in performance mirroring the evolution of structural properties towards the bulk material.

#### 4. Discussion

Bulk elemental analysis and spectroscopic data strongly suggest that 4 is derived from the melon motif (3) (Fig. 1). However, surface analysis by XPS and TEM/EDX indicates that some surface carbonization occurred during pyrolysis. The composites 5 – 7 exhibit very similar IR and NMR data to 4, although elemental analysis of 5 – 7 is consistent with either increased condensation towards g-C<sub>3</sub>N<sub>4</sub>, or increased carbonization over the oxide support; XPS and TEM/EDX suggest that CN@mac-SiO<sub>2</sub> contains more carbonaceous material than 4, with low cyanamide concentrations consistent with a graphitic-like material, as reported for various type of graphitic, graphene, graphene oxide or simply amorphous carbons.[81-85] Nevertheless, the predominant carbon-containing phase of 5 – 7 is CN, and based on elemental analysis (Table 1) the approximate bulk carbonaceous content is 6 wt% compared to less than 2 % for 4. As all compounds and composites were prepared under identical

conditions, the implication is that the oxide support mediates partial decomposition of cyanamide, or its condensation products, to carbonaceous material.

TEM shows that the distribution of CN species in **5 – 7** is inhomogeneous, supported by DRUVS which indicates modification of the periodic photonic structure of mac-SiO<sub>2</sub>, notably by higher CN concentrations, implicating their incorporation in-pore and consistent with the small loss in surface area compared to mac-SiO<sub>2</sub>. Collectively our results show that CN sheets/carbonaceous material penetrate the macropore structure, which hinders their aggregation and the formation of a bulk melon phase, and also partially coats the external mac-SiO<sub>2</sub> surface.

With respect to the photocatalytic reactivity, the rate of hydrogen production of Pt-**4** is ca. 200 μmol h<sup>-1</sup> g<sup>-1</sup>, which is typical of other carbon nitride/melon materials prepared from hydrocarbon precursors at 500 - 600 °C with 3% Pt loading.[26, 36, 42, 80] Composites Pt-**5 - 7** show an inverse relationship between CN content and specific activity, which is potentially a consequence of the higher specific surface area of CN species, formation of more catalytically active sites, and/or suppression of excited state recombination. These possibilities are now discussed below.

With respect to specific surface area, higher rates of hydrogen production have been reported for other platinized carbon nitride morphologies compared to equivalent bulk CN materials. These include mesoporous,[35-37, 39-41, 45, 48, 86] nanocluster,[49, 52] and nanosheet[42-44] structures with surface areas spanning 60 - 400 m<sup>2</sup> g<sup>-1</sup>, although there is no linear correlation between surface area and photocatalytic hydrogen production.[41] For example, mesoporous carbon nitrides exhibit maximum activity around 70 m<sup>2</sup> g<sup>-1</sup>, with further increases in surface area reducing hydrogen production;[36] the activity of such mesoporous morphologies is approximately 8 times that of bulk carbon nitride, despite a 30-fold increase in surface area. Other morphologies also exhibit enhanced hydrogen production: 9-fold for nanoclusters,[49] exfoliated nanosheets[42] and macro- to nano-hierarchical structures;[50] and 3-fold for nanorods[46]. Composites **5 - 7** have lower areas than some mesoporous and nanostructured carbon nitrides, however the CN component could conceivably account for a large fraction of the surface area measured by N<sub>2</sub> adsorption if the porous walls of the mac-SiO<sub>2</sub> support were heavily decorated with CN. However, CO<sub>2</sub> chemisorption (Table 1) shows that the specific surface area of the CN component is very similar for **5 – 7** indicating that the differences in photoactivity between composites cannot be ascribed to surface area. Furthermore, the high specific activity of Pt-**5 – 7** is strongly suggestive of photoactivity throughout the macroporous structure, and not confined to the outer, low external area surfaces of the particles.

The composition and defect structure of carbon nitride are also known to influence photocatalytic activity, as illustrated by comparison of highly crystalline melem (**2**) and melon (prepared under an autogenous pressure of ammonia) which show very low activity.[25] In contrast, low molecular weight melem oligomers prepared under an inert atmosphere are up to six times more active than melon analogues.[25] Related high temperature routes between 520 – 640 °C gave materials with superior photoactivity, attributed to the distribution of imino/amino defects[87] and range of oligomerization. Post-synthetic modification can also alter defect concentration. For example, melon delamination under hydrogen at 550 °C introduces defects that increase photoactivity.[88] The implication from these literature reports is that terminal groups promote (photocatalytic) hydrogen production. For our composites **5 – 7**, the CN concentration renders characterization challenging. <sup>13</sup>C CP-MAS NMR shows little difference in the local structures of CN within **4 - 7** which all contain terminal imino/amino groups. IR data also do not show clear distinguishing features. However, the surface sensitive XPS data (Fig. 5) reveals the presence of significant carbonaceous and terminal cyanide species for **5 - 7**, notably for the lower CN concentrations **5** and **6**, where interactions with the silica support are greatest, suggesting that CN surfaces in **5 – 7** possess higher defect concentrations than **4**. CO<sub>2</sub> temperature programmed desorption of **5 – 7** (Fig. S7) does show clear differences in desorption temperatures indicating a progression of increasingly basic sites from **5** to **7**, suggesting that less basic sites promote greater photocatalytic activity. Although it has been proposed that less basic sites are due to pyridyl-like and more basic sites to amino-like groups, respectively[18] clear-cut assignment is uncertain.

With respect to excited state recombination, defects and carbonaceous material may alter both recombination mechanism(s) and rate. Several examples of CN composites with carbonaceous materials are reported to exhibit enhanced photoactivity relative to ‘pure’ carbon nitride. These include graphene, graphene oxide, polyanilines, carbon nanotubes, and carbon quantum dots, spanning amorphous to crystalline microstructures.[17, 60, 89-92] Rate enhancement is commonly attributed to decreased recombination due to interfacial heterojunction formation. However, excited state lifetimes for carbon nitrides are generally short, with charge carrier largely confined to a tris-*s*-triazine ring restricting their diffusion lengths.[88, 93-99] [98] Indeed, increased photoactivity has been observed for modified carbon nitrides with faster relaxation rates than unmodified carbon nitride, wherein superior photoactivity was attributed to improved catalysis.[88] In light of these previous observations, steady state and time-resolved photoluminescence were acquired for **4 - 7** to probe emission and excited state recombination rates. Steady state emission maps of **4 – 7**

are shown in Fig. S10a. Emission data for **4** and **7** are very similar to that reported for melon and related carbon nitriles prepared above 550 °C, which show excitation and emission maxima centred at 400 and 480 nm, respectively.[88, 93-99] [98] In contrast, composites **5** and **6** give blue-shifted emission and excitation (350 and 460 nm for **5**), with the spectra for **6** particularly broad. Results for **5** and **6** are consistent with CN materials produced at lower temperature, where condensation is less complete than for **4** and **7**, indicative of more oligomeric species.[98] Time-resolved photoluminescence spectroscopy supports this hypothesis (Fig. 8). Materials **4–7** exhibit exponential decay, as observed for other carbon nitride materials and their derivatives.[93, 94, 96-98] Spectral fitting required multi-exponential functions, consistent with multiple relaxation processes, with **4–7** giving excellent fits for the most common tri-exponential function (Table 3). Literature values for the average lifetimes of carbon nitride materials prepared from hydrocarbon precursors are several ns. For **5 - 7** the average lifetimes were between 4.96 and 7.60 ns, versus 13.27 ns for **4**, implying that the excited state lifetime of mac-SiO<sub>2</sub> supported CN is shortened due to faster recombination rates. This is consistent with increased charge trapping at defect sites or heterojunctions present as a result of the terminal CN/CNH<sub>x</sub> and carbonaceous species observed in CN@mac-SiO<sub>2</sub> materials.

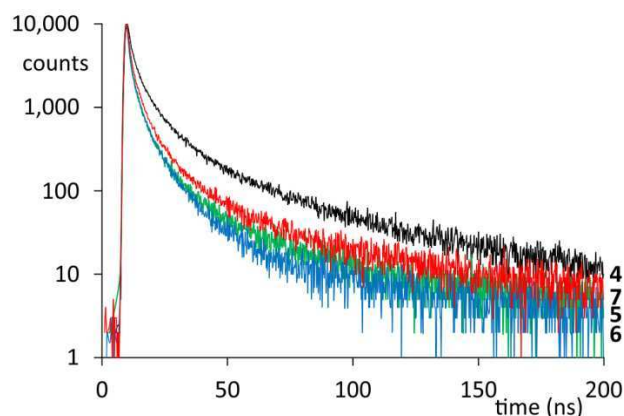


**Fig. 8.** Time-resolved photoluminescence decay curves for bulk CN (**4**) and CN@mac-SiO<sub>2</sub> (**5 – 7**).

**Table 3.** Time constants ( $\tau$ ), relative contribution (%), and average lifetime ( $\tau_{ave}$ ) derived from time-resolved photoluminescence spectroscopy of bulk CN (**4**) and CN@mac-SiO<sub>2</sub> (**5 – 7**).

Sample	$\tau_1$ (ns):(%)	$\tau_2$ (ns):(%)	$\tau_3$ (ns):(%)	$\tau_{ave}$ (ns)
<b>4</b>	1.41±0.03(29)	7.13±0.12(43)	34.93±0.58(28)	13.27±0.22
<b>5</b>	0.68±0.01(40)	4.35±0.06(43)	24.49±0.46(16)	6.11±0.11
<b>6</b>	0.56±0.01(38)	3.99±0.06(45)	17.88±0.33(16)	4.96±0.08
<b>7</b>	0.87±0.02(37)	4.89±0.07(44)	27.43±0.01(18)	7.60±0.04

Finally, the photonic structure of the mac-SiO<sub>2</sub> host could increase light absorption via slow photon effects at the stop band edges or scattering.[6-9] However, since there is only a small refractive index difference between SiO<sub>2</sub> (1.45), and the photocatalytic medium (water (1.00) and triethanolamine (1.48)), the optical properties of the periodic macroporous structure are unlikely to strongly modify light absorption and consequent hydrogen production.

In summary, our results indicate that the structure of CN in **5** – **7** depends on the initial concentration of cyanamide deposited onto mac-SiO<sub>2</sub>, which in turn regulates photocatalytic activity. For **5** – **7**, cyanamide condensation results in compounds based on the melon motif, but is accompanied by greater carbonization than observed for **4**. Spectroscopic data suggests that less condensation, or reduced aggregation of melon units (e.g. via hydrogen bonding) occurs for **5** and **6** in comparison to **4** and **7**, in other words, the density of defects/edge sites appears to decrease with cyanamide loading across the series **5** – **7**. Chemisorption data also shows that **5** – **7** exhibit different distributions of available basic sites and that higher photocatalytic activity is associated with weaker basic sites. In this respect, **5** and **7** are representative of carbon nitrides obtained via ‘low’ and ‘high’ temperature condensation respectively. Adsorption on mac-SiO<sub>2</sub> therefore modifies condensation and aggregation presumably by restricting the mobility of condensing CN oligomers. The role, if any, of the carbonaceous component in controlling photocatalysis is hard to deconvolute, but is clearly not responsible for increasing excited state lifetimes, as previously noted for other carbon nitride/carbon composites,[17, 60, 89-92] and hence rate enhancements are unlikely to originate through improved charge separation. A direct catalytic role for the carbonaceous material cannot be discounted, however the limited impact on charge separation suggests that this component is not directly responsible for the increased photoactivity of composites versus bulk CN. Overall, the superior photocatalytic performance of the composite photocatalysts likely reflects the formation of a higher density of catalytically active sites due to incomplete condensation and aggregation of carbon nitrides than improved charge transport properties.

## **5. Conclusions**

Porous composites derived from the carbon nitride melon created in-situ within a mac-SiO<sub>2</sub> architecture are excellent photocatalysts for the sacrificial production of hydrogen under visible light irradiation. The mac-SiO<sub>2</sub> structure facilitates the dispersion of CN sheets, which are primarily melon-like in structure, preventing their bulk aggregation and concomitant loss of surface area, and affords a high density of catalytically active terminal

CN/CNH sites. The support also promotes partial carbonization of cyanamide and its derivatives, which is of relevance to many porous and nanostructured CN materials prepared using silica templates. While such carbonaceous ‘impurities’ have been shown in the literature to play an important role in enhancing photocatalytic activity, the underpinning mechanism in our composites does not appear linked to improved rates of electron-hole recombination and requires further elucidation through further spatially-resolved electron and X-ray microscopic and time-resolved spectroscopic investigations.

## Acknowledgements

The authors thank The University of York and the Wild Fund for studentship support (S.Q.). Characterization data was enabled via support from the EPSRC-funded Leeds EPSRC Nanoscience and Nanotechnology Equipment Facility (LENNF)(EP/K023853/1), and EPSRC grant awards EP/K029525/2 and EP/K021796/1.

## Appendix A. Supplementary data

Supplementary data related to this article can be found at .....

## References

- [1] H. Kisch, *Semiconductor Photocatalysis*. Wiley-VCH Verlag GmbH: Weinheim, 2015; p 264.
- [2] J. M. Thomas, W. J. Thomas, *Principles and Practice of Heterogeneous Catalysis*. Wiley-VCH Verlag GmbH: Weinheim, 2014; p 768.
- [3] X. F. Yang, A. Q. Wang, B. T. Qiao, J. Li, J. Y. Liu, T. Zhang, Single-Atom Catalysts: A New Frontier in Heterogeneous Catalysis. *Accounts Chem. Res.* (2013), **46**, 1740-1748.
- [4] S. L. Wegener, T. J. Marks, P. C. Stair, Design Strategies for the Molecular Level Synthesis of Supported Catalysts. *Accounts Chem. Res.* (2012), **45**, 206-214.
- [5] J. Regalbuto, *Catalyst Preparation: Science and Engineering*. CRC Press: Boca Raton, FL, 2006; p 488.
- [6] A. Imhof, W. L. Vos, R. Sprik, A. Lagendijk, Large dispersive effects near the band edges of photonic crystals. *Phys. Rev. Lett.* (1999), **83**, 2942-2945.
- [7] J. I. L. Chen, G. von Freymann, V. Kitaev, G. A. Ozin, Effect of disorder on the optically amplified photocatalytic efficiency of titania inverse opals. *J. Am. Chem. Soc.* (2007), **129**, 1196-1202.
- [8] X. Q. Chen, J. H. Ye, S. X. Ouyang, T. Kako, Z. S. Li, Z. G. Zou, Enhanced Incident Photon-to-Electron Conversion Efficiency of Tungsten Trioxide Photoanodes Based on 3D-Photonic Crystal Design. *ACS Nano* (2011), **5**, 4310-4318.

- [9] M. El Harakeh, L. Halaoui, Enhanced Conversion of Light at TiO<sub>2</sub> Photonic Crystals to the Blue of a Stop Band and at TiO<sub>2</sub> Random Films Sensitized with Q-CdS: Order and Disorder. *J. Phys. Chem. C* (2010), **114**, 2806-2813.
- [10] B. Konig, *Chemical Photocatalysis*. De Gruyter: Berlin, 2013; p 400.
- [11] N. Zhang, Y. H. Zhang, Y. J. Xu, Recent progress on graphene-based photocatalysts: current status and future perspectives. *Nanoscale* (2012), **4**, 5792-5813.
- [12] G. C. Xie, K. Zhang, B. D. Guo, Q. Liu, L. Fang, J. R. Gong, Graphene-Based Materials for Hydrogen Generation from Light-Driven Water Splitting. *Adv. Mater.* (2013), **25**, 3820-3839.
- [13] J. W. Chen, J. W. Shi, X. Wang, H. J. Cui, M. L. Fu, Recent progress in the preparation and application of semiconductor/graphene composite photocatalysts. *Chin. J. Catal.* (2013), **34**, 621-640.
- [14] H. X. Wang, Q. Wang, K. G. Zhou, H. L. Zhang, Graphene in Light: Design, Synthesis and Applications of Photo-active Graphene and Graphene-Like Materials. *Small* (2013), **9**, 1266-1283.
- [15] H. Q. Sun, S. B. Wang, Research Advances in the Synthesis of Nanocarbon-Based Photocatalysts and Their Applications for Photocatalytic Conversion of Carbon Dioxide to Hydrocarbon Fuels. *Energy Fuels* (2014), **28**, 22-36.
- [16] S. Y. Lim, W. Shen, Z. Q. Gao, Carbon quantum dots and their applications. *Chem. Soc. Rev.* (2015), **44**, 362-381.
- [17] J. Liu, Y. Liu, N. Y. Liu, Y. Z. Han, X. Zhang, H. Huang, et al., Metal-free efficient photocatalyst for stable visible water splitting via a two-electron pathway. *Science* (2015), **347**, 970-974.
- [18] J. J. Zhu, P. Xiao, H. L. Li, S. A. C. Carabineiro, Graphitic Carbon Nitride: Synthesis, Properties, and Applications in Catalysis. *ACS Appl. Mater. Interfaces* (2014), **6**, 16449-16465.
- [19] X. J. Lang, X. D. Chen, J. C. Zhao, Heterogeneous visible light photocatalysis for selective organic transformations. *Chem. Soc. Rev.* (2014), **43**, 473-486.
- [20] B. V. Lotsch, M. Doblinger, J. Sehnert, L. Seyfarth, J. Senker, O. Oeckler, et al., Unmasking melon by a complementary approach employing electron diffraction, solid-state NMR spectroscopy, and theoretical calculations-structural characterization of a carbon nitride polymer. *Chem. Eur. J.* (2007), **13**, 4969-4980.
- [21] A. V. Semench, L. N. Blinov, Theoretical prerequisites, problems, and practical approaches to the preparation of carbon nitride: A Review. *Glass Phys. Chem.* (2010), **36**, 199-208.
- [22] A. Thomas, A. Fischer, F. Goettmann, M. Antonietti, J. O. Muller, R. Schlogl, et al., Graphitic carbon nitride materials: variation of structure and morphology and their use as metal-free catalysts. *J. Mater. Chem.* (2008), **18**, 4893-4908.
- [23] S. Dyjak, W. Kicinski, A. Huczko, Thermite-driven melamine condensation to C<sub>x</sub>N<sub>y</sub>H<sub>z</sub> graphitic ternary polymers: towards an instant, large-scale synthesis of g-C<sub>3</sub>N<sub>4</sub>. *J. Mater. Chem. A* (2015), **3**, 9621-9631.
- [24] A. Schwarzer, T. Saplinova, E. Kroke, Tri-s-triazines (s-heptazines)-From a "mystery molecule" to industrially relevant carbon nitride materials. *Coord. Chem. Rev.* (2013), **257**, 2032-2062.

- [25] V. W. H. Lau, M. B. Mesch, V. Duppel, V. Blum, J. Senker, B. V. Lotsch, Low-Molecular-Weight Carbon Nitrides for Solar Hydrogen Evolution. *J. Am. Chem. Soc.* (2015), **137**, 1064-1072.
- [26] X. C. Wang, K. Maeda, A. Thomas, K. Takanabe, G. Xin, J. M. Carlsson, et al., A metal-free polymeric photocatalyst for hydrogen production from water under visible light. *Nat. Mater.* (2009), **8**, 76-80.
- [27] X. C. Wang, S. Blechert, M. Antonietti, Polymeric Graphitic Carbon Nitride for Heterogeneous Photocatalysis. *Acs Catal.* (2012), **2**, 1596-1606.
- [28] M. Kawaguchi, K. Nozaki, Synthesis, Structure, and Characteristics of the New Host Material  $(C_3N_3)_2(NH)_3$  (N). *Chem. Mat.* (1995), **7**, 257-264.
- [29] T. Tyborski, C. Merschjann, S. Orthmann, F. Yang, M. C. Lux-Steiner, T. Schedel-Niedrig, Crystal structure of polymeric carbon nitride and the determination of its process-temperature-induced modifications. *J. Phys-Condens. Mat.* (2013), **25**.
- [30] S. Matsumoto, E. Q. Xie, F. Izumi, On the validity of the formation of crystalline carbon nitrides,  $C_3N_4$ . *Diam. Relat. Mat.* (1999), **8**, 1175-1182.
- [31] L. Seyfarth, J. Seyfarth, B. V. Lotsch, W. Schnick, J. Senker, Tackling the stacking disorder of melon-structure elucidation in a semicrystalline material. *Phys. Chem. Chem. Phys.* (2010), **12**, 2227-2237.
- [32] E. Kroke,  $g-C_3N_4$ -The First Stable Binary Carbon(IV) Nitride. *Angew. Chem. Int. Ed.* (2014), **53**, 11134-11136.
- [33] J. H. Li, B. A. Shen, Z. H. Hong, B. Z. Lin, B. F. Gao, Y. L. Chen, A facile approach to synthesize novel oxygen-doped  $g-C_3N_4$  with superior visible-light photoreactivity. *Chem. Commun.* (2012), **48**, 12017-12019.
- [34] P. Niu, L. C. Yin, Y. Q. Yang, G. Liu, H. M. Cheng, Increasing the Visible Light Absorption of Graphitic Carbon Nitride (Melon) Photocatalysts by Homogeneous Self-Modification with Nitrogen Vacancies. *Adv. Mater.* (2014), **26**, 8046.
- [35] X. F. Chen, Y. S. Jun, K. Takanabe, K. Maeda, K. Domen, X. Z. Fu, et al., Ordered Mesoporous SBA-15 Type Graphitic Carbon Nitride: A Semiconductor Host Structure for Photocatalytic Hydrogen Evolution with Visible Light. *Chem. Mat.* (2009), **21**, 4093-4095.
- [36] X. C. Wang, K. Maeda, X. F. Chen, K. Takanabe, K. Domen, Y. D. Hou, et al., Polymer Semiconductors for Artificial Photosynthesis: Hydrogen Evolution by Mesoporous Graphitic Carbon Nitride with Visible Light. *J. Am. Chem. Soc.* (2009), **131**, 1680.
- [37] K. Kailasam, J. D. Epping, A. Thomas, S. Losse, H. Junge, Mesoporous carbon nitride-silica composites by a combined sol-gel/thermal condensation approach and their application as photocatalysts. *Energy Environ. Sci.* (2011), **4**, 4668-4674.
- [38] Y. Zheng, J. Liu, J. Liang, M. Jaroniec, S. Z. Qiao, Graphitic carbon nitride materials: controllable synthesis and applications in fuel cells and photocatalysis. *Energy Environ. Sci.* (2012), **5**, 6717-6731.
- [39] L. C. Jia, H. Q. Wang, D. Dhawale, C. Anand, M. A. Wahab, Q. M. Ji, et al., Highly ordered macro-mesoporous carbon nitride film for selective detection of acidic/basic molecules. *Chem. Commun.* (2014), **50**, 5976-5979.

- [40] Z. K. Zhao, Y. T. Dai, J. H. Lin, G. R. Wang, Highly-Ordered Mesoporous Carbon Nitride with Ultrahigh Surface Area and Pore Volume as a Superior Dehydrogenation Catalyst. *Chem. Mat.* (2014), **26**, 3151-3161.
- [41] X. B. Li, A. F. Masters, T. Maschmeyer, Photocatalytic Hydrogen Evolution from Silica-Templated Polymeric Graphitic Carbon Nitride-Is the Surface Area Important? *ChemCatChem* (2015), **7**, 121-126.
- [42] S. B. Yang, Y. J. Gong, J. S. Zhang, L. Zhan, L. L. Ma, Z. Y. Fang, et al., Exfoliated Graphitic Carbon Nitride Nanosheets as Efficient Catalysts for Hydrogen Evolution Under Visible Light. *Adv. Mater.* (2013), **25**, 2452-2456.
- [43] P. Niu, L. L. Zhang, G. Liu, H. M. Cheng, Graphene-Like Carbon Nitride Nanosheets for Improved Photocatalytic Activities. *Adv. Funct. Mater.* (2012), **22**, 4763-4770.
- [44] K. Schwinghammer, M. B. Mesch, V. Duppel, C. Ziegler, J. Senker, B. V. Lotsch, Crystalline Carbon Nitride Nanosheets for Improved Visible-Light Hydrogen Evolution. *J. Am. Chem. Soc.* (2014), **136**, 1730-1733.
- [45] Y. J. Cui, J. S. Zhang, G. G. Zhang, J. H. Huang, P. Liu, M. Antonietti, et al., Synthesis of bulk and nanoporous carbon nitride polymers from ammonium thiocyanate for photocatalytic hydrogen evolution. *J. Mater. Chem.* (2011), **21**, 13032-13039.
- [46] X. H. Li, J. S. Zhang, X. F. Chen, A. Fischer, A. Thomas, M. Antonietti, et al., Condensed Graphitic Carbon Nitride Nanorods by Nanoconfinement: Promotion of Crystallinity on Photocatalytic Conversion. *Chem. Mat.* (2011), **23**, 4344-4348.
- [47] X. J. Bai, T. Cao, C. B. Cao, Macroporous Carbon Nitride: Synthesis, Loading with Metal Nanoparticles and Catalytic Activity. *Sci. Adv. Mater.* (2012), **4**, 1007-1012.
- [48] J. Liang, Y. Zheng, J. Chen, J. Liu, D. Hulicova-Jurcakova, M. Jaroniec, et al., Facile Oxygen Reduction on a Three-Dimensionally Ordered Macroporous Graphitic C<sub>3</sub>N<sub>4</sub>/Carbon Composite Electrocatalyst. *Angew. Chem. Int. Ed.* (2012), **51**, 3892-3896.
- [49] J. Liu, J. H. Huang, D. Dontosova, M. Antonietti, Facile synthesis of carbon nitride micro-/nanoclusters with photocatalytic activity for hydrogen evolution. *RSC Adv.* (2013), **3**, 22988-22993.
- [50] Y. S. Jun, J. Park, S. U. Lee, A. Thomas, W. H. Hong, G. D. Stucky, Three-Dimensional Macroscopic Assemblies of Low-Dimensional Carbon Nitrides for Enhanced Hydrogen Evolution. *Angew. Chem. Int. Ed.* (2013), **52**, 11083-11087.
- [51] M. K. Bhunia, K. Yamauchi, K. Takanebe, Harvesting Solar Light with Crystalline Carbon Nitrides for Efficient Photocatalytic Hydrogen Evolution. *Angew. Chem. Int. Ed.* (2014), **53**, 11001-11005.
- [52] J. S. Zhang, M. W. Zhang, C. Yang, X. C. Wang, Nanospherical Carbon Nitride Frameworks with Sharp Edges Accelerating Charge Collection and Separation at a Soft Photocatalytic Interface. *Adv. Mater.* (2014), **26**, 4121-4126.
- [53] Y. Zheng, L. H. Lin, X. J. Ye, F. S. Guo, X. C. Wang, Helical Graphitic Carbon Nitrides with Photocatalytic and Optical Activities. *Angew. Chem. Int. Ed.* (2014), **53**, 11926-11930.

- [54] T. P. Ang, Sol-gel synthesis of a novel melon-SiO<sub>2</sub> nanocomposite with photocatalytic activity. *Catal. Commun.* (2009), **10**, 1920-1924.
- [55] T. P. Ang, Y. M. Chan, Comparison of the Melon Nanocomposites in Structural Properties and Photocatalytic Activities. *J. Phys. Chem. C* (2011), **115**, 15965-15972.
- [56] M. Shalom, S. Inal, D. Neher, M. Antonietti, SiO<sub>2</sub>/carbon nitride composite materials: The role of surfaces for enhanced photocatalysis. *Catal. Today* (2014), **225**, 185-190.
- [57] L. Y. Huang, H. Xu, Y. P. Li, H. M. Li, X. N. Cheng, J. X. Xia, et al., Visible-light-induced WO<sub>3</sub>/g-C<sub>3</sub>N<sub>4</sub> composites with enhanced photocatalytic activity. *Dalton Trans.* (2013), **42**, 8606-8616.
- [58] L. Y. Huang, Y. P. Li, H. Xu, Y. G. Xu, J. X. Xia, K. Wang, et al., Synthesis and characterization of CeO<sub>2</sub>/g-C<sub>3</sub>N<sub>4</sub> composites with enhanced visible-light photocatalytic activity. *RSC Adv.* (2013), **3**, 22269-22279.
- [59] P. Xiao, Y. X. Zhao, T. Wang, Y. Y. Zhan, H. H. Wang, J. L. Li, et al., Polymeric Carbon Nitride/Mesoporous Silica Composites as Catalyst Support for Au and Pt Nanoparticles. *Chem. Eur. J.* (2014), **20**, 2872-2878.
- [60] Z. W. Zhao, Y. J. Sun, F. Dong, Graphitic carbon nitride based nanocomposites: a review. *Nanoscale* (2015), **7**, 15-37.
- [61] R. Mitchell, R. Brydson, R. E. Douthwaite, Homogeneous coating of photonic macroporous oxides with inorganic nanocrystals. *Nanoscale* (2014), **6**, 4043-4046.
- [62] R. C. Schroden, M. Al-Daous, C. F. Blanford, A. Stein, Optical properties of inverse opal photonic crystals. *Chem. Mat.* (2002), **14**, 3305-3315.
- [63] S. Brunauer, P. H. Emmett, E. Teller, Adsorption of gases in multimolecular layers. *J. Am. Chem. Soc.* (1938), **60**, 309-319.
- [64] R. Mitchell, R. Brydson, R. E. Douthwaite, Enhancement of hydrogen production using photoactive nanoparticles on a photochemically inert photonic macroporous support. *Phys. Chem. Chem. Phys.* (2015), **17**, 493-499.
- [65] J. Liebig, Uber Einige Stickstoff - Verbindungen. *Ann. Pharm.* (1834), **10**, 1-47.
- [66] F. Goettmann, A. Fischer, M. Antonietti, A. Thomas, Chemical Synthesis of Mesoporous Carbon Nitrides Using Hard Templates and Their Use as a Metal-Free Catalyst for Friedel-Crafts Reaction of Benzene. *Angew. Chem. Int. Ed.* (2006), **45**, 4467-4471.
- [67] M. Groenewolt, M. Antonietti, Synthesis of g-C<sub>3</sub>N<sub>4</sub> Nanoparticles in Mesoporous Silica Host Matrices. *Adv. Mater.* (2005), **17**, 1789-1792.
- [68] T. Cherdhirankorn, M. Retsch, U. Jonas, H. J. Butt, K. Koynov, Tracer Diffusion in Silica Inverse Opals. *Langmuir* (2010), **26**, 10141-10146.
- [69] D. G. Gong, J. G. Highfield, S. Z. E. Ng, Y. X. Tang, W. C. J. Ho, Q. L. Tay, et al., Poly Tri-s-triazines as Visible Light Sensitizers in Titania-Based Composite Photocatalysts: Promotion of Melon Development from Urea over Acid Titanates. *ACS Sustain. Chem. Eng.* (2014), **2**, 149-157.

- [70] A. Stein, B. E. Wilson, S. G. Rudisill, Design and functionality of colloidal-crystal-templated materials-chemical applications of inverse opals. *Chem. Soc. Rev.* (2013), **42**, 2763-2803.
- [71] L. Gonzalez-Urbina, K. Baert, B. Kolaric, J. Perez-Moreno, K. Clays, Linear and Nonlinear Optical Properties of Colloidal Photonic Crystals. *Chem. Rev.* (2012), **112**, 2268-2285.
- [72] F. Marlow, Muldarisnur, P. Sharifi, R. Brinkmann, C. Mendive, Opals: Status and Prospects. *Angew. Chem. Int. Ed.* (2009), **48**, 6212-6233.
- [73] Y. X. Zhao, B. F. Yang, J. Xu, Z. P. Fu, M. Wu, F. Li, Facile synthesis of Ag nanoparticles supported on TiO<sub>2</sub> inverse opal with enhanced visible-light photocatalytic activity. *Thin Solid Films* (2012), **520**, 3515-3522.
- [74] Q. Li, J. P. Yang, D. Feng, Z. X. Wu, Q. L. Wu, S. S. Park, et al., Facile synthesis of porous carbon nitride spheres with hierarchical three-dimensional mesostructures for CO<sub>2</sub> capture. *Nano Research* (2010), **3**, 632-642.
- [75] S. M. Lyth, Y. Nabaie, S. Moriya, S. Kuroki, M. Kakimoto, J. Ozaki, et al., Carbon Nitride as a Nonprecious Catalyst for Electrochemical Oxygen Reduction. *J. Phys. Chem. C* (2009), **113**, 20148-20151.
- [76] V. N. Khabashesku, J. L. Zimmerman, J. L. Margrave, Powder synthesis and characterization of amorphous carbon nitride. *Chem. Mat.* (2000), **12**, 3264-3270.
- [77] D. Foy, G. Demazeau, P. Florian, D. Massiot, C. Labrugere, G. Goglio, Modulation of the crystallinity of hydrogenated nitrogen-rich graphitic carbon nitrides. *J. Solid State Chem.* (2009), **182**, 165-171.
- [78] K. Schwinghammer, B. Tuffy, M. B. Mesch, E. Wirnhier, C. Martineau, F. Taulelle, et al., Triazine-based Carbon Nitrides for Visible-Light-Driven Hydrogen Evolution. *Angew. Chem. Int. Ed.* (2013), **52**, 2435-2439.
- [79] K. Zhang, L. J. Guo, Metal sulphide semiconductors for photocatalytic hydrogen production. *Catalysis Science & Technology* (2013), **3**, 1672-1690.
- [80] K. Maeda, X. C. Wang, Y. Nishihara, D. L. Lu, M. Antonietti, K. Domen, Photocatalytic Activities of Graphitic Carbon Nitride Powder for Water Reduction and Oxidation under Visible Light. *J. Phys. Chem. C* (2009), **113**, 4940-4947.
- [81] D. R. Dreyer, S. Park, C. W. Bielawski, R. S. Ruoff, The chemistry of graphene oxide. *Chem. Soc. Rev.* (2010), **39**, 228-240.
- [82] M. A. Ali, S. Srivastava, P. R. Solanki, V. Reddy, V. V. Agrawal, C. Kim, et al., Highly Efficient Bionzyme Functionalized Nanocomposite-Based Microfluidics Biosensor Platform for Biomedical Application. *Sci Rep* (2013), **3**, 9.
- [83] B. Kumar, M. Asadi, D. Pisasale, S. Sinha-Ray, B. A. Rosen, R. Haasch, et al., Renewable and metal-free carbon nanofibre catalysts for carbon dioxide reduction. *Nat. Commun.* (2013), **4**, 8.
- [84] N. Daems, X. Sheng, I. F. J. Vankelecom, P. P. Pescarmona, Metal-free doped carbon materials as electrocatalysts for the oxygen reduction reaction. *J. Mater. Chem. A* (2014), **2**, 4085-4110.
- [85] J. Gorka, R. T. Mayes, L. Baggetto, G. M. Veith, S. Dai, Sonochemical functionalization of mesoporous carbon for uranium extraction from seawater. *J. Mater. Chem. A* (2013), **1**, 3016-3026.

- [86] G. H. Dong, L. Z. Zhang, Porous structure dependent photoreactivity of graphitic carbon nitride under visible light. *J. Mater. Chem.* (2012), **22**, 1160-1166.
- [87] P. Wu, J. R. Wang, J. Zhao, L. J. Guo, F. E. Osterloh, Structure defects in g-C<sub>3</sub>N<sub>4</sub> limit visible light driven hydrogen evolution and photovoltage. *J. Mater. Chem. A* (2014), **2**, 20338-20344.
- [88] X. B. Li, G. Hartley, A. J. Ward, P. A. Young, A. F. Masters, T. Maschmeyer, Hydrogenated Defects in Graphitic Carbon Nitride Nanosheets for Improved Photocatalytic Hydrogen Evolution. *J. Phys. Chem. C* (2015), **119**, 14938-14946.
- [89] F. He, G. Chen, Y. G. Yu, S. Hao, Y. S. Zhou, Y. Zheng, Facile Approach to Synthesize g-PAN/g-C<sub>3</sub>N<sub>4</sub> Composites with Enhanced Photocatalytic H<sub>2</sub> Evolution Activity. *ACS Appl. Mater. Interfaces* (2014), **6**, 7171-7179.
- [90] Q. J. Xiang, J. G. Yu, M. Jaroniec, Preparation and Enhanced Visible-Light Photocatalytic H<sub>2</sub>-Production Activity of Graphene/C<sub>3</sub>N<sub>4</sub> Composites. *J. Phys. Chem. C* (2011), **115**, 7355-7363.
- [91] A. Suryawanshi, P. Dhanasekaran, D. Mhamane, S. Kelkar, S. Patil, N. Gupta, et al., Doubling of photocatalytic H<sub>2</sub> evolution from g-C<sub>3</sub>N<sub>4</sub> via its nanocomposite formation with multiwall carbon nanotubes: Electronic and morphological effects. *Int. J. Hydrog. Energy* (2012), **37**, 9584-9589.
- [92] G. Z. Liao, S. Chen, X. Quan, H. T. Yu, H. M. Zhao, Graphene oxide modified g-C<sub>3</sub>N<sub>4</sub> hybrid with enhanced photocatalytic capability under visible light irradiation. *J. Mater. Chem.* (2012), **22**, 2721-2726.
- [93] H. Y. Zhang, A. C. Yu, Photophysics and Photocatalysis of Carbon Nitride Synthesized at Different Temperatures. *J. Phys. Chem. C* (2014), **118**, 11628-11635.
- [94] C. Merschjann, T. Tyborski, S. Orthmann, F. Yang, K. Schwarzburg, M. Lublow, et al., Photophysics of polymeric carbon nitride: An optical quasimonomer. *Phys. Rev. B* (2013), **87**, 8.
- [95] J. Chen, S. H. Shen, P. H. Guo, P. Wu, L. J. Guo, Spatial engineering of photo-active sites on g-C<sub>3</sub>N<sub>4</sub> for efficient solar hydrogen generation. *J. Mater. Chem. A* (2014), **2**, 4605-4612.
- [96] J. Chen, S. H. Shen, P. Wu, L. J. Guo, Nitrogen-doped CeOx nanoparticles modified graphitic carbon nitride for enhanced photocatalytic hydrogen production. *Green Chem.* (2015), **17**, 509-517.
- [97] Y. Huang, Y. J. Wang, Y. Q. Bi, J. R. Jin, M. F. Ehsan, M. Fu, et al., Preparation of 2D hydroxyl-rich carbon nitride nanosheets for photocatalytic reduction of CO<sub>2</sub>. *RSC Adv.* (2015), **5**, 33254-33261.
- [98] Y. H. Zhang, Q. W. Pan, G. Q. Chai, M. R. Liang, G. P. Dong, Q. Y. Zhang, et al., Synthesis and luminescence mechanism of multicolor-emitting g-C<sub>3</sub>N<sub>4</sub> nanopowders by low temperature thermal condensation of melamine. *Sci Rep* (2013), **3**, 8.
- [99] Y. W. Yuan, L. L. Zhang, J. Xing, M. I. B. Utama, X. Lu, K. Z. Du, et al., High-yield synthesis and optical properties of g-C<sub>3</sub>N<sub>4</sub>. *Nanoscale* (2015), **7**, 12343-12350.